Supporting Information

Synthesis of Interface-Driven Tunable Bandgap Metal Oxides

Boyce S. Chang,[1] Andrew Martin,[1] Brijith Thomas,[2,3] Ang Li,[4] Rick W. Dorn,[2,3] Jinlong Gong,[4] Aaron J. Rossini,[2,3*] Martin M. Thuo[1,5,6*]

[1]Department of Materials Science & Engineering, Iowa State University, 528 Bissell road. Ames, IA 50011, USA

[2]Department of Chemistry, Iowa State University. Ames, IA 50011, USA

[3]US DOE Ames Laboratory

[4]School of Chemical Engineering & Technology, Tianjin University, 135 Yaguan road. Tianjin 300350, China

[5]Department of Electrical & Computer Engineering, Iowa State University, 2520 Osborn Drive. Ames, IA 50011, USA

[6]Microelectronics Research Center, 133 Applied Sciences Complex I, 1925 Scholl Road, Ames, Iowa 50011, United States

Experimental Procedures

Materials: Glacial acetic (99.7%) was purchased from Fisher Scientific, eutectic gallium-indium (99.99%) was purchased from Sigma Aldrich and ethanol (>99.2%) was purchased from Decon Laboratories.

Methods

Synthesis of Ga-based coordination polymer. EGaIn liquid metal particles were synthesized using the SLICE method.[1] The particle size ranged between 1 – 50 μm. For a typical synthesis, 2 g of EGaIn particles was suspended 40 ml acetic acid solution (5% v/v, pH = 3.8). After several weeks, the precipitates (coordination polymer) were purified by ethanol and/or acetone washing through centrifugation and filtration. Complete conversion of the metal was typically attained.

Heat treatment. 2 g of Ga-based coordination polymer was placed into a closed ceramic crucible. The crucible was subsequently inserted into a tube furnace set to the target temperature for 2 hours.

Anaerobic heat treatment is performed using a sealed tube that is subsequently evacuated for 60 seconds prior to insertion into the tube furnace. Pressure in the tube is approximately 13 Pa, resulting in oxygen partial pressure of ~3 Pa. Data points collected at 370˚C were initially set to 400 ˚C, however, due to inaccuracy of the attached thermocouple in this range, temperature was corrected using an infrared thermometer.

Scanning electron microscopy. High resolution SEM images of the heat-treated materials were obtained using a FEI Helios NanoLab G3 UC under immersion mode at 1 kV accelerating voltage. Images of the pristine coordination polymer was obtained using an FEI Quanta 250 at 1 kV accelerating voltage with backscattered detector.

Transmission electron microscopy. High resolution TEM images of the heat-treated materials were obtained using a Jeol JSM-2100F Field Emission Electron Microscope at 200 kV accelerating voltage.

Thermogravimetric analysis coupled differential scanning calorimetry, infrared spectroscopy, and mass spectroscopy. TGA-DSC-IR-MS was performed using a Netzsch STA449 F1 with ramp rate of 20 °C min^{-1}, under argon atmosphere. The evolved gases were analyzed by FTIR using Bruker Tensor 37 (liquid nitrogen cooled) and mass spectroscopy using Netzsch QMS 403D. The materials were analyzed from 40 °C to 800 °C. Thermally induced mass drift was mitigated by subtracting the spectra with a blank run.

UV-vis spectroscopy. Samples were mixed in powdered KCl salt using mortar and pestle. The mixture was then compressed in a mold *in vacuo* to form a pellet. UV-vis absorption was performed using an Agilent 8453 Diode Array UV-Vis.

Nitrogen sorption. All sorption experiments were performed using Micromeritics ASAP 2020 with ultra-high purity nitrogen gas. Samples were first heated *in vacuo* for 6 hours at 120°C, before transferring for analysis.

Powder X-ray diffraction. A Rigaku Smartlab X-ray diffractometer with Cu K-alpha radiation was used to perform all powder X-ray diffraction experiments.

Solid-state nuclear magnetic resonance. The acetic acid gallium coordination polymer heat-treated at 370 °C was analyzed by both fast MAS room temperature solid-state NMR spectroscopy and DNP-enhanced solid-state NMR spectroscopy. The sample for DNP-enhanced solid-state NMR experiments was prepared by gently grinding by hand in a mortar and pestle for approximately half a minute. 20 mg of the ground heat-treated coordination polymer was impregnated with 15 μL of a DNP polarizing agent solution. [2] The polarizing agent solution consisted of the nitroxide biradical TEKPol with a concentration of 15 mM in the solvent tetrachloroethane (TCE).[3] The impregnated sample was then packed into a sapphire 3.2 mm rotor and capped with a polytetrafluoroethylene insert and a zirconia drive cap.

DNP-enhanced solid-state NMR experiments were performed on a Bruker 9.4 T 400 MHz/263 GHz DNP solid-state NMR spectrometer equipped with a Bruker Avance III console.[4] The main magnetic field-sweep coil was set to give optimum ^{1}H DNP enhancement with TEKPol

as the polarizing agent. A 3.2 mm double resonance DNP probe was used for acquisition of the DNP-enhanced NMR spectra. The MAS frequency of the DNP experiment was approximately 10 kHz, and sample temperature was around 110 K. [1] H chemical shifts were referenced with respect to neat tetramethylsilane by setting the chemical shift of the frozen tetrachloroethane ^{1}H NMR signal to 6.2 ppm. Cross-polarization (CP) ^{1}H→^{13}C NMR spectra were obtained with a rotor synchronized CP spin echo pulse sequence with the spin echo lasting two rotor cycles in duration. The CP contact time was 2 ms. The MAS modified Hartmann-Hahn match condition was directly optimized on the sample and used ^{1}H and ^{13}C spin-lock pulses with RF fields of 87 kHz and 24 kHz, respectively. SPINAL-64 heteronuclear decoupling was applied with a ^{1}H RF field of 100 kHz. [5] The ^{1}H→^{13}C CP spin echo NMR spectra shown in Figure 3f were acquired with 5000 scans and a 3 s recycle delay.

Room temperature solid-state NMR experiments were performed on a 9.4 T Bruker wide-bore magnet equipped with a Bruker Avance III HD spectrometer. MAS experiments were performed using either a (Figure 2) Bruker 1.3 mm HX probe at a MAS rate of 50 kHz or a (Figure S2) Bruker 2.5 mm HXY probe configured in double resonance mode at a MAS rate of 25 kHz.[6] ^{1}H and ^{13}C chemical shifts were referenced to neat tetramethylsilane via an external secondary standard of adamantane (δ_{iso} = 1.82 ppm). [7] ^{71}Ga chemical shifts were referenced with respect to proton chemical shifts by the recommended relative frequency scale. [7] ^{13}C spin echo solid state NMR spectra at 25 and 50 kHz MAS was collected with a rotor synchronized spin echo pulse sequence ($\pi/2 - \tau_r - \pi - \tau_r$). The $\pi/2$ and π pulses were either 2.5 μs and 5.0 μs or 3.125 μs and 6.25 μs for experiments performed at 50 and 25 kHz MAS, respectively. The proton detected ^{1}H{^{13}C}[8] CP-HETCOR spectrum was obtained with the previously described pulse sequence.[9] The forwards and backwards CP steps employed a contact time of 2.5 ms. Residual ^{1}H magnetization after the

forwards CP step was removed by applying 0.3 ms of ^{1}H pulses with the RF field set to 25 kHz to fulfill the HORROR condition. During the indirect dimension ^{13}C chemical shift evolution ^{1}H heteronuclear decoupling was performed with 25 kHz continuous wave decoupling to satisfy the HORROR condition. The t_1-evolution period was incremented in steps of 40 μs, corresponding to an indirect spectral width of 25 kHz hypercomplex indirect dimension points were obtained. 16 scans were obtained for each t_1-increment and the recycle delay was 0.7 s (56 minutes total experiment time). The STATES-TPPI procedure was used to achieve sign discrimination and obtain absorptive peaks in the indirect dimension. 1D ^{1}H→^{13}C CPMAS experiments (Figure S2) were performed with either 80 μs or 1 ms of CP and a 25 kHz MAS frequency. CP was achieved with a ^{1}H radio frequency (RF) field of *ca.* 70 kHz and a ^{13}C RF field of *ca.* 40 kHz. A 90-100 % linear ramp was applied to the ^{1}H channel during the CP spin-lock to broaden the Hartman-Hahn match condition. ^{1}H heteronuclear decoupling (100 kHz RF using the SPINAL-64 sequence)[5] was performed during the acquisition of ^{13}C. Static ^{71}Ga SSNMR spectra were acquired with the QCPMG pulse sequence. ^{71} Ga pulse widths were calibrated with a 1.0 M aqueous solution of $GaCl_3$. Continuous wave ^{1}H hetero-nuclear decoupling with a rf field of 50 kHz was applied for the duration of the static QCPMG experiments. The static ^{71}Ga SSNMR spectrum of pristine is obtained using WURST- QCPMG pulse and of 370°C, 800°C and 1000°C treated samples were acquired with a rotor synchronized QCPMG pulse sequence. The ^{71}Ga SSNMR spectrum of the pristine was acquired with 25 μs WURST pulses with a total frequency sweep width of 600 kHz and a single transmitter offset. The central transition selective π/2 and π pulses were in the range

of 0.6 μs and 1.2 μs, respectively. Echo reconstructed static ^{71}Ga SSNMR spectra were formed from the CPMG spectra by co-adding each of the spin echoes in the CPMG echo-train together, then Fourier transforming the resulting whole spin echo.

Table S1. The parameters used for acquiring the QCPMG spectra.

	1000	**800**	**370**	**pristine**
spin echoes	96	96	96	40
π/2	0.6 μs	0.6 μs	0.79 μs	0.6 μs
π	1.2 μs	1.2 μs	1.59 μs	1.2 μs
ns	8192	4096	8192	1128
recycle delay	0.25 s	0.63 s	0.25 s	0.5 s

Raman Spectroscopy. Anaerobic heat-treated Ga oxide at 600˚C was spread on the coverslip and checked by a Horiba XploRA Raman microscope (HORIBA Scientific, Edison, NJ). A 532 nm laser (1.24 mW) and a 50X (0.5 NA) long working distance objective was used to collect the Raman spectrum for the sample with 30s acquisition for 3 accumulations. The Raman spectrum shown was an average of spectrum for 10 random locations.

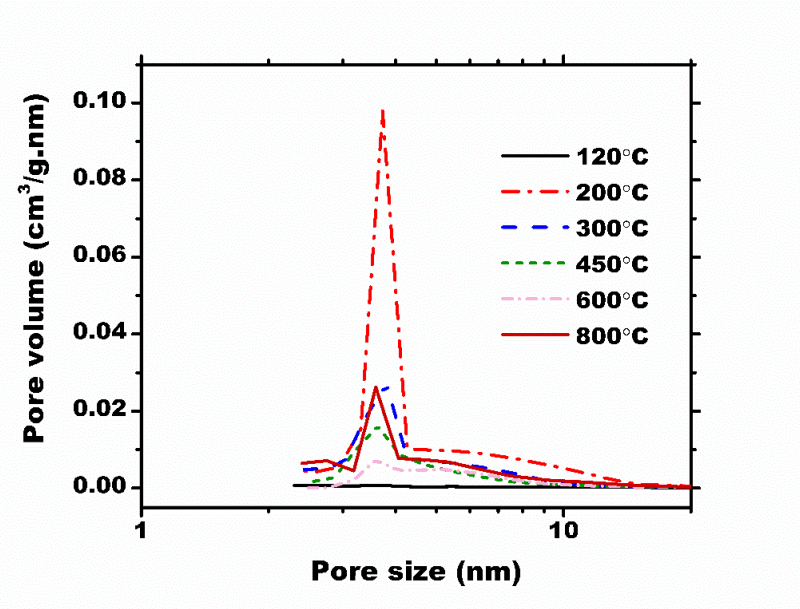

Figure S1. Pore size distribution of nanobeams at varying heat treatment temperature.

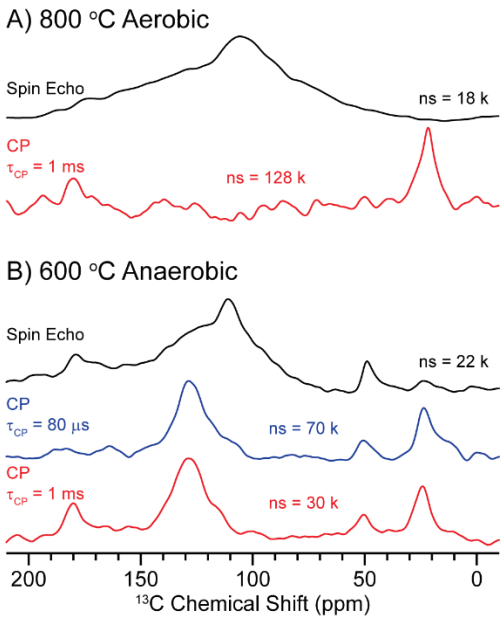

Figure S2. 1D (black) direct excitation ^{13}C and (red and blue) $^{1}H \rightarrow ^{13}C$ CPMAS solid-state NMR spectra of the Ga nanobeam sample treated to (A) 800 °C under aerobic conditions and (B) 600 °C under anaerobic conditions. CP contact times were either (blue) 80 µs or (red) 1 ms in duration. Number of scans (ns) used to record all spectra are given in the figure.

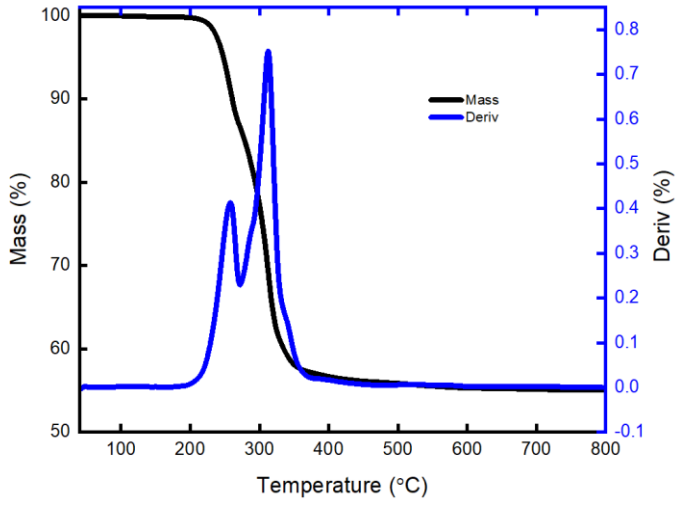

Figure S3. Thermogravimetric analysis of In-based coordination polymer.

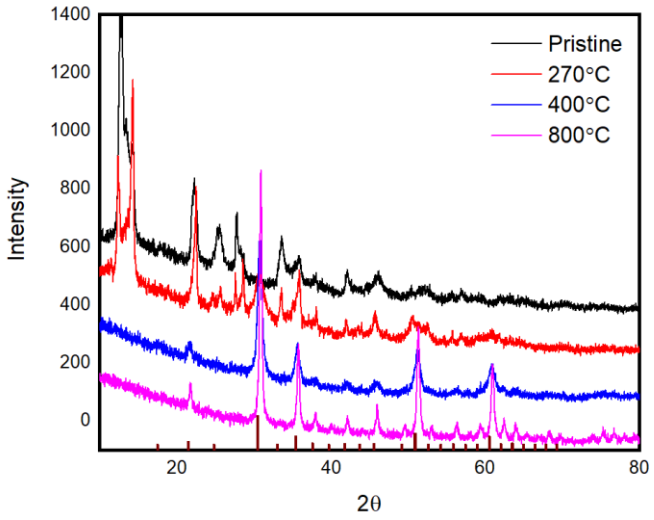

Figure S4. Powder X-ray diffraction In-based coordination polymer (pristine) heat treated to various temperatures.

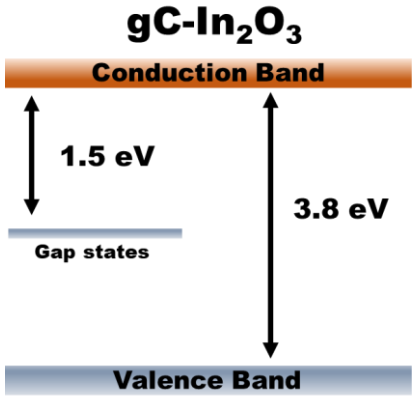

Figure S5. Optical transitions in gC-In_2O_3. Graphite induced gap states significantly improves absorption of low energy photons.

Photocatalytic CO_2 reduction. The home-made photocatalytic reactor consisted of a sealed chamber, an embedded window made by quartz glass and a liquid sampling port sealed by a silicone pad. The reactor was connected to a gas circulation system with a ten-port value (VICI) for on-line sampling to a gas chromatograph (Ruimin GC 2060, Shanghai). The gas circulation

system was prima[8]rily made of stainless steel tubing and a home-made gas pump for the circulation of the gas. A mechanical pump was connected into the system to exhaust the carrier gas of the gas chromatograph when switch back the ten-port value. A pressure gauge was also connected into the system to monitor the gas pressure. The total volume of the gas in the circulation system after filling the reactor with electrolyte was 80 mL.

Before the start of reaction, 0.05 g of catalyst was mixed in the reactor with 30 mL of an aqueous solution of $KHCO_3$ (0.1M, to enhance the solubility of CO_2) and Na_2SO_3 (0.1M, to act as a hole sacrifice agent). Then, the system was evacuated to remove air. Subsequently, the suspension in reactor was purged with CO_2 (≥ 99.995%) for 1 h to achieve CO_2 saturation and the initial CO_2 pressure was kept at atmospheric pressure. There was no more CO_2 purged into the closed system during the reaction. The gases in the closed circulation system were continuously circulated through the suspension for the entire reaction period. The reactions were carried out under 100 mW/cm^2 UV illumination (wavelength <420 nm).

The analysis of the gaseous reaction mixtures containing CO, CH_4, H_2, was carried out using a gas chromatograph, which was equipped with a TCD, FID and a methanizer which contained a Ni catalyst. Argon (≥ 99.999%) was used as the carrier gas. The back channel of GC was equipped with two packed columns, TDX-01 and Molsieve 5 Å, and two gas switch valves. During the analysis, 1.0 mL of gas sample in the sample loop of ten-port value was introduced to the TDX-01 column where CO_2 was separated from the other gases due to its longer retention time. The rest of the gases after the TDX-01 column was further separated by the Molsieve 5 Å column. The gas product of H_2 was detected by TCD and CH_4, CO were further detected by FID with higher sensitivities. The role of the methanizer was to convert CO to CH_4 for FID analysis.

Table S2. Unpaired semiconductor catalyst used for CO_2 reduction in H_2O.

Catalyst	CH_4 (μmol/g.h)	Other (μmol/g.h)	Radiation
β-Ga_2O_3 (This work)	23	189 (CO)	Xe (<420 nm)
β-Ga_2O_3[11]	<1	2 (CO)	Xe
Nafion-Pd-TiO_2[12]	17	Trace (C_2H_6)	Xe
Ni-TiO_2[13]	14	N.A.	UV (365 nm)
Pt-TiO_2[14]	11	Trace (CO)	Xe
$W_{18}O_{49}$[15]	11	N.A.	Xe (>420 nm)
Ti-β Zeolite[16]	6	1 (CH_3OH)	Hg (>250 nm)
HNb_3O_8[17]	4	N.A.	Xe

Table S3. Major products from proton assisted reduction of CO_2 at standard conditions.[10]

Reaction	**E^0**
$2H_2O + 2e^- \rightarrow 2OH^- + H_2$	–0.41
$CO_2 + 2H^+ + 2e^- \rightarrow CO + H_2O$	–0.51
$CO_2 + 2H^+ + 2e^- \rightarrow HCOOH$	–0.58
$2CO_2 + 2H^+ + 2e^- \rightarrow H_2C_2O_4$	–0.87
$CO_2 + 6H^+ + 6e^- \rightarrow CH_3OH + H_2O$	–0.39
$CO_2 + 8H^+ + 8e^- \rightarrow CH_4 + 2H_2O$	–0.24
$2CO_2 + 12H^+ + 12e^- \rightarrow C_2H_5OH + 3H_2O$	–0.33
$2CO_2 + 14H^+ + 14e^- \rightarrow C_2H_6 + 4H_2O$	–0.27

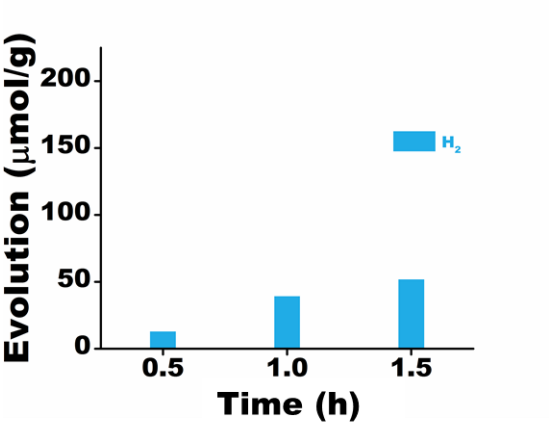

Figure S6. Hydrogen evolution reaction (HER) in 40% methanol aqueous solution.

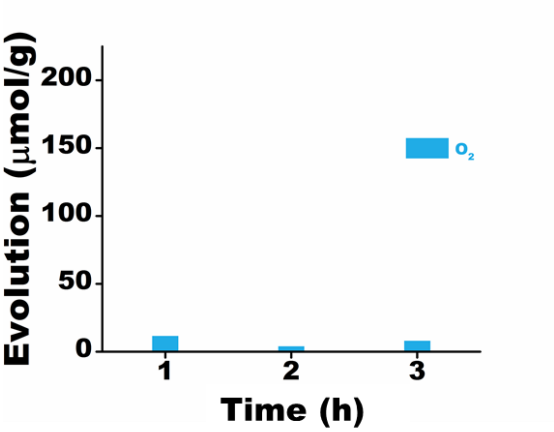

Figure S7. Oxygen evolution reaction (OER) in 30% $NaIO_3$ aqueous solution.

References

1. Tevis, I. D.; Newcomb, L. B.; Thuo, M., Synthesis of Liquid Core-Shell Particles and Solid Patchy Multicomponent Particles by Shearing Liquids Into Complex Particles (SLICE). *Langmuir* **2014,** *30* (47), 14308-14313.

2. Lesage, A.; Lelli, M.; Gajan, D.; Caporini, M. A.; Vitzthum, V.; Miéville, P.; Alauzun, J.; Roussey, A.; Thieuleux, C.; Mehdi, A.; Bodenhausen, G.; Coperet, C.; Emsley, L., Surface Enhanced NMR Spectroscopy by Dynamic Nuclear Polarization. *Journal of the American Chemical Society* **2010,** *132* (44), 15459-15461.

3. Zagdoun, A.; Casano, G.; Ouari, O.; Schwarzwälder, M.; Rossini, A. J.; Aussenac, F.; Yulikov, M.; Jeschke, G.; Copéret, C.; Lesage, A.; Tordo, P.; Emsley, L., Large Molecular Weight Nitroxide Biradicals Providing Efficient Dynamic Nuclear Polarization at Temperatures up to 200 K. *Journal of the American Chemical Society* **2013,** *135* (34), 12790-12797.
4. Rosay, M.; Tometich, L.; Pawsey, S.; Bader, R.; Schauwecker, R.; Blank, M.; Borchard, P. M.; Cauffman, S. R.; Felch, K. L.; Weber, R. T.; Temkin, R. J.; Griffin, R. G.; Maas, W. E., Solid-state dynamic nuclear polarization at 263 GHz: spectrometer design and experimental results. *Physical Chemistry Chemical Physics* **2010,** *12* (22), 5850-5860.
5. Fung, B. M.; Khitrin, A. K.; Ermolaev, K., An Improved Broadband Decoupling Sequence for Liquid Crystals and Solids. *J. Magn. Reson.* **2000,** *142* (1), 97-101.
6. Ishii, Y.; Tycko, R., Sensitivity Enhancement in Solid State 15N NMR by Indirect Detection with High-Speed Magic Angle Spinning. *Journal of Magnetic Resonance* **2000,** *142* (1), 199-204.
7. Morcombe, C. R.; Zilm, K. W., Chemical shift referencing in MAS solid state NMR. *Journal of Magnetic Resonance* **2003,** *162* (2), 479-486.
8. Lefort, R.; Wiench, J. W.; Pruski, M.; Amoureux, J.-P., Optimization of data acquisition and processing in Carr–Purcell–Meiboom–Gill multiple quantum magic angle spinning nuclear magnetic resonance. *The Journal of Chemical Physics* **2002,** *116* (6), 2493-2501.
9. Wiench, J. W.; Bronnimann, C. E.; Lin, V. S. Y.; Pruski, M., Chemical Shift Correlation NMR Spectroscopy with Indirect Detection in Fast Rotating Solids: Studies of Organically Functionalized Mesoporous Silicas. *Journal of the American Chemical Society* **2007,** *129* (40), 12076-12077.
10. Chang, X.; Wang, T.; Gong, J., CO2 photo-reduction: insights into CO2 activation and reaction on surfaces of photocatalysts. *Energy & Environmental Science* **2016,** *9* (7), 2177-2196.
11. Park, H.-a.; Choi, J. H.; Choi, K. M.; Lee, D. K.; Kang, J. K., Highly porous gallium oxide with a high CO2 affinity for the photocatalytic conversion of carbon dioxide into methane. *J. Mater. Chem.* **2012,** *22* (12), 5304-5307.
12. Kim, W.; Seok, T.; Choi, W., Nafion layer-enhanced photosynthetic conversion of CO2 into hydrocarbons on TiO2 nanoparticles. *Energy & Environmental Science* **2012,** *5* (3), 6066-6070.
13. Kwak, B. S.; Vignesh, K.; Park, N.-K.; Ryu, H.-J.; Baek, J.-I.; Kang, M., Methane formation from photoreduction of CO2 with water using TiO2 including Ni ingredient. *Fuel* **2015,** *143*, 570-576.
14. Xie, S.; Wang, Y.; Zhang, Q.; Fan, W.; Deng, W.; Wang, Y., Photocatalytic reduction of CO2 with H2O: significant enhancement of the activity of Pt–TiO2 in CH4 formation by addition of MgO. *Chemical Communications* **2013,** *49* (24), 2451-2453.
15. Xi, G.; Ouyang, S.; Li, P.; Ye, J.; Ma, Q.; Su, N.; Bai, H.; Wang, C., Ultrathin W18O49 Nanowires with Diameters below 1 nm: Synthesis, Near-Infrared Absorption, Photoluminescence, and Photochemical Reduction of Carbon Dioxide. *Angewandte Chemie International Edition* **2012,** *51* (10), 2395-2399.
16. Ikeue, K.; Yamashita, H.; Anpo, M.; Takewaki, T., Photocatalytic Reduction of CO2 with H2O on Ti−β Zeolite Photocatalysts: Effect of the Hydrophobic and Hydrophilic Properties. *The Journal of Physical Chemistry B* **2001,** *105* (35), 8350-8355.
17. Li, X.; Pan, H.; Li, W.; Zhuang, Z., Photocatalytic reduction of CO2 to methane over HNb3O8 nanobelts. *Applied Catalysis A: General* **2012,** *413-414*, 103-108.